Ozone Production and Its Sensitivity to NO_x and VOCs: Results from the DISCOVER-AQ Field Experiment, Houston 2013

Gina M. Mazzuca[1], Xinrong Ren[1,2,*], Christopher P. Loughner[2,3], Mark Estes[4], James H. Crawford[5], Kenneth E. Pickering[1,6], Andrew J. Weinheimer[7], and Russell R. Dickerson[1]

[1]Department of Atmospheric and Oceanic Science, University of Maryland, College Park, MD 20742, USA

[2]Air Resources Laboratory, National Oceanic and Atmospheric Administration, College Park, MD 20740, USA

[3]Earth System Science Interdisciplinary Center, University of Maryland, College Park, MD 20740, USA

[4] Texas Commission on Environmental Quality, Austin, TX 78711, USA

[5] NASA Langley Research Center, Hampton, VA 23681, USA

[6] NASA Goddard Space Flight Center, Greenbelt, MD 20771, USA

[7] National Center for Atmospheric Research, Boulder, CO 80307, USA

*Correspondence to: X. Ren (ren@umd.edu)

Abstract An observation-constrained box model based on the Carbon Bond mechanism, Version 5 (CB05), was used to study photochemical processes along the NASA P-3B flight track and spirals over eight surface sites during the September 2013 Houston, Texas deployment of the NASA DISCOVER-AQ campaign. Data from this campaign provided an opportunity to examine and improve our understanding of atmospheric photochemical oxidation processes related to the formation of secondary air pollutants such as ozone (O_3). O_3 production and its sensitivity to NO_x and VOCs were calculated at different locations and times of day. Ozone production efficiency (OPE), defined as the ratio of the ozone production rate to the NO_x oxidation rate, was calculated using the observations and the simulation results of the box and Community Multiscale Air Quality (CMAQ) models. Correlations of these results with other parameters, such as radical sources and NO_x mixing ratio, were also evaluated. It was generally found that O_3 production tends to be more VOC sensitive in the morning along with high ozone production rates, suggesting that control of VOCs may be an effective way to control O_3 in Houston. In the

afternoon, O_3 production was found to be mainly NO_x sensitive with some exceptions. O_3 production near major emissions sources such as Deer Park was mostly VOC sensitive for the entire day, other urban areas near Moody Tower and Channelview were VOC sensitive or in the transition regime, and areas farther from downtown Houston such as Smith Point and Conroe were mostly NO_x sensitive for the entire day. It was also found that the control of NO_x emissions has reduced O_3 concentrations over Houston, but has led to larger OPE values. The results from this work strengthen our understanding of O_3 production; they indicate that controlling NO_x emissions will provide air quality benefits over the greater Houston metropolitan area in the long run, but in selected areas controlling VOC emissions will also be beneficial.

Keywords Ozone production; Ozone Production Efficiency; Houston; DISCOVER-AQ

1. Introduction

Understanding the non-linear relationship between ozone production and its precursors is critical for the development of an effective ozone (O_3) control strategy. Despite great efforts undertaken in the past decades to address the problem of high ozone concentrations, our understanding of the key precursors that control tropospheric ozone production remains incomplete and uncertain [Molina and Molina, 2004; Xue et al., 2013]. Atmospheric ozone levels are determined by emissions of ozone precursors, atmospheric photochemistry, and transport [Jacob, 1999; Xue et al., 2013]. A major challenge in regulating ozone pollution lies in comprehending its complex and non-linear chemistry with respect to ozone precursors, i.e., nitrogen oxides (NO_x) and volatile organic compounds (VOCs) that varies with time and location (Figure 1). Understanding the non-linear relationship between ozone production and its precursors is critical for the development of an effective ozone control strategy.

Sensitivity of ozone production to NO_x and VOCs represents a major uncertainty for oxidant photochemistry in urban areas [Sillman et al., 1995; 2003]. In urban environments, ozone is formed through photochemical processes when its precursors NO_x and VOCs are emitted into the atmosphere from many sources. Depending on physical and chemical conditions, the production of ozone can be either NO_x-sensitive or VOC-sensitive due to the complexity of these photochemical processes. Therefore, effective ozone control strategies rely heavily on the accurate understanding of how ozone responds to reduction of NO_x and VOC emissions, usually

63 simulated by photochemical air quality models [e.g., Sillman et al., 2003; Lei et al., 2004; Mallet
64 and Sportisse, 2005; Li et al, 2007; Chen et al., 2010; Tang et al., 2010; Xue et al., 2013;
65 Goldberg et al., 2016]. However, those model-based studies have inputs or parameters subject to
66 large uncertainties that can affect not only the simulated levels of ozone but also the ozone
67 dependence on its precursors.

68 There are some observation-based studies of ozone production and its relationships with
69 NO_x and VOCs [e.g., Thielmann et al., 2002; Zaveri et al., 2003; Ryerson et al., 2003; Griffin et
70 al., 2003; Kleinman et al., 2005a; Neuman et al., 2009; Mao et al., 2010; Ren et al., 2013]. Using
71 in-situ aircraft observations, Kleinman et al. [2005a] studied five U.S. cities and found that ozone
72 production rates vary from nearly zero to 155 ppb hr^{-1} with differences depending on the
73 concentration of ozone precursors NOx and VOCs. They also found that in Houston, NO_x and
74 light olefins are co-emitted from petrochemical facilities leading to the highest ozone production
75 of the five cities [Kleinman et al., 2005a]. Using the data collected at a single surface location
76 during the Study of Houston Atmospheric Radical Precursors (SHARP) in spring 2009, the
77 temporal variation of O_3 production was observed: VOC-sensitive in the early morning and NO_x-
78 sensitive for most of the afternoon [Ren et al., 2013]. This is similar to the behavior observed in
79 two previous summertime studies in Houston: the Texas Air Quality Study in 2000 (TexAQS
80 2000) and the TexAQS II Radical and Aerosol Measurement Project in 2006 (TRAMP 2006)
81 [Mao et al., 2010; Chen et al., 2010]. In a more recent study using measurements in four cities in
82 China, ozone production was found to be in a VOC-sensitive regime in both Shanghai and
83 Guangzhou, but in a mixed regime in Lanzhou [Xue et al., 2013]. In the work presented here, we
84 provide investigations of spatial and temporal variations of ozone production and its sensitivity
85 to NOx and VOCs to provide a scientific basis to develop a non-uniform emission reduction
86 strategy for O_3 pollution control in urban and suburban areas such as the greater Houston
87 metropolitan area.

88 This work utilized observations made during the Deriving Information on Surface
89 Conditions from COlumn and VERtically Resolved Observations Relevant to Air Quality
90 (DISCOVER-AQ) campaign in Houston in September 2013. This field campaign is unique due
91 to the comprehensive air sampling performed over a large spatial (urban and suburban areas in
92 and around Houston) and temporal (entire month of September 2013) range. Measurements were
93 collected from various platforms including the National Aeronautics and Space Administration

(NASA) P-3B and B-200 aircraft, ground surface sites, and mobile laboratories. Eight surface monitoring stations (Smith Point, Galveston, Manvel Croix, Deer Park, Channelview, Conroe, West Houston, and Moody Tower) were selected where the P-3B conducted vertical spirals (Figure 2) [DISCOVER-AQ whitepaper].

2. Methods

2.1 Ozone production Scenarios and Sensitivity

During the day, the photochemical O_3 production rate is essentially the production rate of NO_2 molecules from HO_2 + NO and RO_2 + NO reactions [Finlayson-Pitts and Pitts, 2000]. The net instantaneous photochemical O_3 production rate, $P(O_3)$, can be written approximately as the following equation:

$$P(O_3) = k_{HO_2+NO}[HO_2][NO] + \sum k_{RO_{2i}+NO}[RO_{2i}][NO] - k_{OH+NO_2+M}[OH][NO_2][M] - P(RONO_2)$$
$$-k_{HO_2+O_3}[HO_2][O_3] - k_{OH+O_3}[OH][O_3] - k_{O(^1D)+H_2O}[O(^1D)][H_2O] - L(O_3 + alkenes) \quad (1)$$

where, *k term*s are the reaction rate coefficients; RO_{2i} is the individual organic peroxy radicals. The negative terms in Eq. (1) correspond to the reaction of OH and NO_2 to form nitric acid, the formation of organic nitrates, $P(RONO_2)$, the reactions of OH and HO_2 with O_3, the photolysis of O_3 followed by the reaction of $O(^1D)$ with H_2O, and O_3 reactions with alkenes. Ozone is additionally destroyed by dry deposition.

The dependence of O_3 production on NO_x and VOCs can be categorized into two typical scenarios: NO_x sensitive and VOC sensitive. The method proposed by Kleinman [2005b] was used to evaluate the O_3 production sensitivity using the ratio of L_N/Q, where L_N is the radical loss via the reactions with NO_x and Q is the total primary radical production. Because the radical production rate is approximately equal to the radical loss rate, this L_N/Q ratio represents the fraction of radical loss due to NO_x. It was found that when L_N/Q is significantly less than 0.5, the atmosphere is in a NO_x-sensitive regime, and when L_N/Q is significantly greater than 0.5, the atmosphere is in a more VOC-sensitive regime [Kleinman et al., 2001; Kleinman, 2005b]. Note that the contribution of organic nitrates impacts the cut-off value for L_N/Q to determine the ozone production sensitivity to NO_x or VOCs and this value may vary slightly around 0.5 in different environments [Kleinman, 2005b].

2.2 Box Model Simulations

An observation-constrained box model with the Carbon Bond Mechanism Version 2005 (CB05) was used to simulate the oxidation processes in Houston during DISCOVER-AQ. Measurements made on the P-3B were used as input to constrain the box model. From the box model results, the ozone production rate and its sensitivity to NO_x and VOCs were calculated allowing us to calculate ozone production efficiency at different locations and at different times of day.

CB05 is a well-known chemical mechanism that has been actively used in research and regulatory applications [Yarwood et al., 2005]. Organic species are lumped according to the carbon bond approach, that is, bond type, e.g., carbon single bond and double bond. Reactions are aggregated based on the similarity of carbon bond structure so that fewer surrogate species are needed in the model. Some organics (e.g., organic nitrates and aromatics) are lumped. The lifetime of alkyl nitrates is too long in CB05 and has been corrected in CB6r2 [Canty et al., 2015], but this should have minimal impact on our findings because the model is constrained to observations as indicated below.

The box model was run using measurements, including long-lived inorganic and organic compounds and meteorological parameters (temperature, pressure, humidity, and photolysis frequencies), from the NASA P-3B. One-minute archived data were used as model input (available at http://www-air.larc.nasa.gov/missions/discover-aq/discover-aq.html). The model ran for 24 hours for each data point to allow most calculated reactive intermediates to reach steady state, but short enough to prevent the buildup of secondary products. An additional lifetime of two days was assumed for some calculated long-lived species such as organic acids and alcohols to avoid unexpected accumulation of these species in the model. At the end of 24 hours, the model generated time series of OH, HO_2, RO_2, and other reactive intermediates. The box model simulations covered the entire P-3B flight track during DISCOVER-AQ, including the eight science sites where the P-3B conducted spirals. Note that unlike a three-dimensional chemical transport model, the zero-dimensional box model simulations did not include advection and emissions. Although advection and emissions are certainly important factors for the air pollution formation, they can be omitted in the box model since all of the long-lived radical and O_3 precursors were measured and used to constrain the box model calculations. The box model

155 analysis is necessary for ozone production and its sensitivity to NO_x and VOCs because the box
156 model was constrained to measured species (e.g., NO, NO_2, CO, HCHO, etc.) and
157 meteorological parameters (e.g., photolysis frequencies) that are essential to calculate ozone
158 production rates. Even though there is good agreement in general between the box model and
159 the 3D model, there are still some differences between the measurements and the output from the
160 3D model that are shown below, e.g., NOx, CO, HCHO and photolysis frequencies.
161
162 **2.3 WRF-CMAQ Model Simulations**
163 The WRF model was run from 18 August 2013 to 1 October 2013 with nested domains
164 with horizontal resolutions of 36, 12, 4, and 1 km and 45 vertical levels. This work utilized
165 results from the 4 km domain. The modeling domains are shown in Figure 3. WRF was run
166 straight through (i.e., was not re-initialized at all) using an iterative technique developed at the
167 EPA and described in Appel et al. (2014). Observational and analysis nudging were performed
168 on all domains. Model output was saved hourly for the 36 and 12 km domains, every 20 minutes
169 for the 4 km domain, and every 5 minutes for the 1 km domain. WRF and CMAQ configuration
170 options and inputs are shown in Table 1.
171 WRF model results were used to drive the CMAQ model offline. The 2012 baseline
172 anthropogenic emissions from the Texas Commission on Environmental Quality (TCEQ) were
173 used as input to CMAQ. These emissions contain the most-up-to-date Texas anthropogenic
174 emissions inventory and a compilation of emissions estimates from Regional Planning Offices
175 throughout the US. Biogenic emissions were calculated online within CMAQ with Biogenic
176 Emission Inventory System (BEIS). Lightning emissions were also calculated online within
177 CMAQ. CMAQ was run with the process analysis tool to output ozone production rate ($P(O_3)$),
178 ozone loss rate ($L(O_3)$), and net ozone production rate (net $P(O_3)$) as well as ozone production
179 efficiency (OPE).
180
181 **3. RESULTS**
182 **3.1 Photochemical O_3 Production Rate, Sensitivity, and Diurnal Variations**
183 Figure 4 shows the net ozone production rate, net $P(O_3)$, calculated using the box model
184 results along the P-3B flight track for all flight days during the Houston deployment. There are
185 several $P(O_3)$ hotspots over the Houston Ship Channel located to the east/southeast of downtown

Houston as well as downwind, over Galveston Bay. This is expected because of large emissions of NO_x and VOCs from the Houston Ship Channel, where the highest $P(O_3)$ was observed – up to ~140 ppbv hr^{-1}. $P(O_3)$ values up to ~80-90 ppbv hr^{-1} were observed over Galveston Bay, mainly on September 25, 2013, consistent with high ozone levels observed across the Houston area on that day. Similar instantaneous ozone production rates have been observed in two previous studies in Houston in 2000 and 2006 [Kleinman et al., 2002a; Mao et al., 2010].

Figure 5 shows the indicator L_N/Q of ozone production sensitivity along the P-3B flight track for all flight days during the Houston deployment. $P(O_3)$ was mainly VOC-sensitive over the Houston Ship Channel and its surrounding urban areas due to large NO_x emissions. Over areas away from the center of the city with relatively low NO_x emissions, $P(O_3)$ was usually NOx-sensitive. Vertical profiles of $P(O_3)$, $L(O_3)$, and net ozone production calculated using the box model results (Figure 6) show that:

(1) $RO_2 + NO$ makes about the same amount of O_3 as $HO_2 + NO$ in the model;

(2) O_3 photolysis followed by $O(^1D)+H_2O$ is a dominant process for the photochemical ozone loss;

(3) the maximum net $P(O_3)$ appeared near the surface below 1 km.

In the diurnal variations of $P(O_3)$, a broad peak in the morning with significant $P(O_3)$ in the afternoon was obtained on ten flight days during DISCOVER-AQ in Houston (Figure 7). High $P(O_3)$ mainly occurred with $L_N/Q > 0.5$ (i.e., in the VOC sensitive regime). The diurnal variation of L_N/Q indicates that $P(O_3)$ was mainly VOC sensitive in the early morning and then transitioned towards the NO_x sensitive regime later in the day (Figure 8). High $P(O_3)$ in the morning was mainly associated with VOC sensitivity due to high NO_x levels in the morning (points in the red circle in Figure 8). Although $P(O_3)$ was mainly NO_x sensitive in the afternoon between 12:00 and 17:00 Central Standard Time, CST (UTC-6 hours), there were also periods and locations when $P(O_3)$ was VOC sensitive, e.g., the points with $L_N/Q > 0.5$ between 12:00 and 17:00 (CST) in Figure 8.

Diurnal variations of ozone production rate at eight individual locations where the P-3B conducted vertical spirals show that the ozone production is greater than 10 ppb hr^{-1} on average at locations with high NO_x and VOC emissions, such as Deer Park, Moody Tower and Channelview, while at locations away from the urban center with lower emissions, such as Galveston, Smith Point, and Conroe, the ozone production usually averaged less than 10 ppb hr^{-1}

(Figure 9). The dependence of $P(O_3)$ on the NO mixing ratio ([NO]) shows that when [NO] is less than ~1 ppbv, ozone production increases as the [NO] increases, i.e., $P(O_3)$ is in NOx sensitive regime. When the NO mixing ratio is greater than ~1 ppbv, ozone production levels off, i.e., $P(O_3)$ is in a NOx saturated regime (Figure 10). It was also found that at a given NO mixing ratio, a higher production rate of HO_x results in a higher ozone production rate. Diurnal variations of the indicator of ozone production sensitivity to NO_x and VOCs, L_N/Q, at eight individual locations where the P-3B conducted vertical spirals show that (1) at Deer Park, $P(O_3)$ was mostly VOC sensitive for the entire day; (2) at Moody Tower and Channelview, $P(O_3)$ was VOC sensitive or in the transition regime; (3) at Smith Point and Conroe, $P(O_3)$ was mostly NOx sensitive for the entire day; and (4) Galveston, West Houston, and Manvel Croix $P(O_3)$ was VOC sensitive only in the early morning (Figure 11).

3.2 Ozone Production Efficiency

Ozone production efficiency (OPE) is defined as the number of molecules of oxidant Ox (= O_3 + NO_2) produced photochemically when a molecule of NO_x (= NO + NO_2) is oxidized. It conveys information about the conditions under which O_3 is formed and is an important parameter to consider when evaluating impacts from NO_x emission sources [Kleinman et al., 2002]. The OPE can be deduced from atmospheric observations as the slope of a graph of O_x concentration versus the concentration of NO_x oxidation products. The latter quantity is denoted as NO_z and is commonly measured as the difference betwUeen NO_y (sum of all reactive-nitrogen compounds) and NO_x, i.e. $NO_z = NO_y - NO_x$.

Figure 12 shows the photochemical oxidant O_x as a function of NO_z during DISCOVER-AQ in Houston in 2013. The two data sets plotted here were collected on September 25 and 26, when high ambient ozone concentrations were observed, and for the data collected during all other flights. Note that the slopes obtained from these two data sets are essentially the same and an average OPE of ~8 is derived from the observations, meaning that 8 molecules of ozone were produced when one molecule of NO_x was consumed. Even though higher ozone concentrations were observed on September 25 and 26, the OPE on these two days are not different from those in other flights, indicating the ozone event on these two days was not caused by a higher OPE, but mainly, by higher concentrations of ozone precursors (and thus higher ozone production rates) and background ozone as indicated by the intercepts in the regression of the two data sets in

Figure 12**.** The high ozone observed on those days could also be due to slower ventilation and different meteorological conditions such as a lower boundary layer height, northerly transport from inland air pollution source regions, stagnant conditions from the high-pressure system, and the bay and gulf breezes.

The OPE value of ~8 during DISCOVER-AQ in Houston in 2013 is greater than the average OPE value obtained during the Texas Air Quality Study in 2006 (TexAQS2006; OPE=5.9±1.2) [Neuman et al., 2009] and TexAQS2000 (OPE=5.4) [Ryerson et al., 2003]. One possible reason for this increased OPE is the continuous reduction in NO_x emissions in Houston from 2000 to 2013 pushed NO_x levels closer to 1 ppbv in 2013 (Figure S1), thus OPE increased since OPE increases as NO_x decreases when the NO_x level is greater than ~1 ppbv (Figure 13).

Houston area OPE values range from about a factor of 1.3 to 2 higher than the OPEs calculated from the DISCOVER-AQ 2011 study in Maryland, likely due to higher photochemical reactivity in Houston (Figure S4). The 2011 Maryland OPEs ranged from 3.4 to 6.1 when all measured data below 1 km are used (Ren, X., unpublished data). An OPE of ~8 was calculated [He et al., 2013] for the 2011 Maryland DISCOVER-AQ campaign for measured data below the 850 hPa level during vertical spirals with a strong linear correlation ($r^2 > 0.8$) between O_x and NO_z. Additionally, OPEs of 7.7-9.7 were obtained from a ground site during the New England Air Quality Study (NEAQS) 2002 (Griffin et al., 2004).

When calculating ozone production efficiency using observed O_x and NO_z, it is important to know whether there is substantial loss of nitric acid (HNO_3), because it can affect the OPE by reducing the NO_z [Trainer et al., 1993; 2000; Neuman et al., 2009] and thus bias the OPE high. The derived OPE in Figure 12 is only valid when there is minimum loss of NO_z (especially HNO_3) from the source region to the point of observations. Neuman et al. [2009] found that $\Delta CO/\Delta NOy$, i.e., the slope in a CO versus NO_y plot, is an indicator for distinguishing plumes with efficient O_3 formation from plumes with similarly high O_3 to NO_x oxidation products correlation slopes caused by variable mixing of aged polluted air depleted in HNO_3. A typical $\Delta CO/\Delta NO_y$ ranges from ~40 in background air to ~4-7 in fresh emission plumes in Houston [Neuman et al., 2009]. The $\Delta CO/\Delta NO_y$ was examined at different times of the day on September 25 and 26. The results indicate that the $\Delta CO/\Delta NO_y$ was about 6.2 (Figure 14a) throughout the day with variation between 6.0 and 7.0 (Figure 14). This demonstrates that the observed O_3

formation was from fresh plumes and was not caused by variable mixing of aged polluted air depleted in HNO_3.

Using both the box model and CMAQ model results, OPE can also be calculated according to its definition, i.e., the net ozone formation rate divided by the formation rate of NO_z. Net $P(O_3)$ was calculated using Eq. (1), while the NO_z formation rate is the sum of HNO_3 and organic nitrate formation rates. The agreement between the box model-derived and the CMAQ-derived OPEs is very good, with the mean OPEs of 14.8±7.4 in the box model and 16.6±8.1 in the CMAQ model. The dependence of OPE on NO_x is also similar for both the box and CMAQ models (Figure 13). On average, the maximum of OPE appears at a NO_x level around 1 ppbv. In general, if the NO_x level is below 1 ppbv, OPE increases as the NO_x level increases, while if the NO_x level is above 1 ppbv, OPE decreases as the NO_x level increases (Figure 13).

The OPE values calculated using the CMAQ and box model are greater than the values derived from the observations using the slope in the scatter plot of Ox versus NO_z in Figure 12. This is expected because in the calculation of OPE using the box and CMAQ model results, a few ozone loss processes, such as ozone dry deposition and horizontal/vertical dispersion, were not considered. This could result in higher calculated ozone production rates using the model results.

Spatial variations of OPE demonstrate that except for a few hotspots over Downtown Houston and the Houston Ship Channel, most large OPEs appear away from the urban center, e.g., the northwest and southeast of the area, while in areas with high NO_x emissions close to the urban center lower OPEs were generally observed (Figure 15). This is again consistent with the results in Figure 13 that the maximum of OPE appears at a NO_x level around 1 ppbv.

4. Discussion and Conclusions

On average, ozone production $P(O_3)$, was about 20-30 ppbv hr^{-1} in the morning and 5-10 ppbv hr^{-1} in the afternoon during DISCOVER-AQ in Houston in 2013. The diurnal variation of $P(O_3)$ shows a broad peak in the morning with significant $P(O_3)$ in the afternoon obtained on ten flight days in September 2013. High $P(O_3)$ mainly occurred with L_N/Q greater than 0.5, i.e., in the VOC sensitive regime. Since $P(O_3)$ depends on NO_x levels and radical production rate, it increases as [NO] increases up to ~1 ppbv and then levels off with further increases of [NO]. At

309 a given [NO], a higher production rate of HO_x results in a higher ozone production rate. This has
310 implications for the NO_x control strategies in order to achieve the ozone control goal.
311 The DISCOVER-AQ campaign in Houston is unique because of its large spatial coverage
312 and thus spatial variations of ozone production and its sensitivity to NOx and VOCs. Diurnal
313 variations of $P(O_3)$ at eight individual locations where the P-3B conducted vertical spirals show
314 that the $P(O_3)$ is on average more than 10 ppbv hr^{-1} at locations with high NO_x and VOC
315 emissions, such as Deer Park, Moody Tower, and Channelview, while at locations away from the
316 urban center with lower emissions of ozone precursors such as Galveston, Smith Point, and
317 Conroe, the ozone production rate is usually less than 10 ppbv hr^{-1} on average. Hotspots of $P(O_3)$
318 were observed over Downtown Houston and the Houston Ship Channel due to significant
319 emissions in these areas.
320 Ozone production tended more towards VOC sensitive in the morning with high $P(O_3)$
321 and in general, NO_x sensitive in the afternoon with some exceptions. It was found that during
322 some afternoon time periods and locations, $P(O_3)$ was VOC sensitive. The diurnal variation of
323 L_N/Q indicates that $P(O_3)$ was mainly VOC sensitive in the early morning and then transitioned
324 towards the NO_x sensitive regime later in the day. High $P(O_3)$ in the morning was mainly
325 associated with VOC sensitivity due to high NO_x levels in the morning. Specifically, Deer Park
326 was mostly VOC sensitive for the entire day, Moody Tower and Channelview were VOC
327 sensitive or in the transition regime, and Smith Point and Conroe were mostly NO_x sensitive for
328 the entire day.
329 Based on the measurements on the P-3B, ozone production efficiency (OPE) was about 8
330 during DISCOVER-AQ 2013 in Houston. This OPE value is greater than the average OPE value
331 (5.9±1.2) obtained during the Texas Air Quality Study in 2006 (TexAQS2006), likely due to the
332 reduction in NO_x emissions in Houston between 2006 and 2013 that pushed NO_x levels closer to
333 1 ppbv in 2013 from higher NOx levels in previous years. The results from this work strengthen
334 our understanding of O_3 production; they indicate that controlling NO_x emissions will provide air
335 quality benefits over the greater Houston metropolitan area in the long run, but in selected areas
336 controlling VOC emissions will also be beneficial.
337
338 **Acknowledgements**

The authors acknowledge the entire DISCOVER-AQ science team for the use of the P-3B measurement data in this work as well as Winston Luke and Paul Kelley at NOAA Air Resources Laboratory for helpful discussion. This work was funded by the Texas Commission on Environmental Quality (TCEQ) through the Air Quality Research Program (AQRP) at University of Texas Austin (Contract #14-020). The contents, findings, opinions, and conclusions are the work of the authors and do not necessarily represent the findings, opinions, or conclusions of the TCEQ or AQRP. NASA AQAST supported RRD.

References

Appel, K.W., Gilliam, R.C., Pleim, J.E., Pouliot, G.A., Wong, D.C., Hogrefe, C., Roselle, S.J., and Mathur, R.: Improvements to the WRF-CMAQ modeling system for fine-scale air quality simulations, EM, 16-21 2014.

Canty, T. P., Hembeck, L., Vinciguerra, T. P. , Anderson, D. C. , Goldberg, D. L. , Carpenter, S. F. , Allen, D. J. , Loughner, C. P. , Salawitch, R. J. , and Dickerson, R. R.: Ozone and NOx chemistry in the eastern US: evaluation of CMAQ/CB05 with satellite (OMI) data, *Atmospheric Chemistry and Physics*, *15*(19), 10965-10982, doi:10.5194/acp-15-10965-2015, 2015.

Chen, S., Ren, X., Mao J., Chen, Z., Brune, W. H., Lefer, B., Rappenglück, B., Flynn J., Olson, J., Crawford, J. H.: A comparison of chemical mechanisms based on TRAMP–2006 field data, Atmos. Environ., 44(33), 4116-4125, 2010.

DISCOVER-AQ whitepaper, http://discover-aq.larc.nasa.gov/pdf/DISCOVER-AQ_science.pdf.

Finlayson-Pitts, B. J., and Pitts, J.: Chemistry of the upper and lower atmosphere: Theory, experiments and applications, Academic Press, San Diego, California, p.264-276, 2000.

Goldberg, D. L., Vinciguerra, T. P., Anderson, D. C., Hembeck, L., Canty, T. P., Salawitch, R. J., and Dickerson, R. R. CAMx Ozone Source Attribution in the Eastern United States using Guidance from Observations during DISCOVER-AQ Maryland, *Geophysical Research Letters*, doi: 10.1002/2015GL067332, 2016.

Griffin, R. J., Johnson, C. A., Talbot, R. W., Mao, H., Russo, R. S., Zhou, Y., and Sive B. C.: Quantification of ozoneformation metrics at Thompson Farm during the New England Air

370 Quality Study (NEAQS) 2002, J. Geophys. Res., 109, D24302,doi:10.1029/2004JD005344,
371 2004.

372 He, H., Hembeck, L., Hosley, K. M., Canty, T. P., Salawitch, R. J., and Dickerson, R. R.: High
373 ozone concentrations on hot days: The role of electric power demand and NOx emissions,
374 Geophys. Res. Lett., 40, 5291–5294, doi:10.1002/grl.50967, 2013.
375
376 Jacob, D. J.: Introduction to Atmospheric Chemistry, Princeton University Press, New Jersey,
377 1999.
378 Kleinman, L. I., Daum, P. H., Lee, Y.-N, Nunnermacker, L. J., Springston, S. R., Weinstein-
379 Lloyd J., and Rudolph, J.: Sensitivity of ozone production rate to ozone precursors. Geophys.
380 Res. Lett., 28, 2903–2906 , doi: 10.1029/2000GL012597, 2001.
381 Kleinman, L. I., Daum, P. H., Lee, Y.-N., Nunnermacker, L. J., Springston, S. R., Weinstein-
382 Lloyd, J., and Rudolph, J.: Ozone production efficiency in an urban area, J. Geophys. Res.,
383 107 (D23), 4733, doi:10.1029/2002JD002529, 2002.
384 Kleinman, L. I., Daum, P. H., Lee, Y.-N., Nunnermacker, L. J., Springston, S. R., Weinstein-
385 Lloyd, J., and Rudolph, J.: A comparative study of ozone production in five U.S.
386 metropolitan areas, J. Geophys. Res., 110, D02301, doi:10.1029/2004JD005096, 2005a.
387 Kleinman, L. I.: The dependence of tropospheric ozone production rate on ozone precursors,
388 Atmos. Environ., 39(3), 575–586, doi:10.1016/j.atmosenv.2004.08.047, 2005b.
389 Lei, W., Zhang, R., Tie, X., and Hess, P.: Chemical characterization of ozone formation in the
390 Houston-Galveston area: A chemical transport model study, J. Geophys. Res., 109, D12301,
391 doi:10.1029/2003JD004219, 2004.
392 Li, G., Zhang, R., Fan, J., and Tie, X.: Impacts of biogenic emissions on photochemical ozone
393 production in Houston, Texas, J. Geophys. Res., 112, D10309, doi:10.1029/2006JD007924,
394 2007.
395 Mallet, V. and Sportisse, B.: A comprehensive study of ozone sensitivity with respect to
396 emissions over Europe with a chemistry-transport model, J. Geophys. Res., 110, D22302,
397 doi:10.1029/2005JD006234, 2005.
398 Mao, J., Ren, X., Chen, S., Brune, W. H., Chen, Z., Martinez, M., Harder, H., Lefer, B.,
399 Rappenglück, B., Flynn, J., and Leuchner, M.: Atmospheric oxidation capacity in the
400 summer of Houston 2006: Comparison with summer measurements in other metropolitan

401 studies, Atmos. Environ., 44(33), 4107-4115, 2010
402 Molina, M. J., and Molina, L. T.: Megacities and atmospheric pollution, J. Air Waste Manage.,
403 54, 644–680, 2004.
404 Neuman, J. A., et al.: Relationship between photochemical ozone production and NOx oxidation
405 in Houston, Texas, J. Geophys. Res., 114, D00F08, doi:10.1029/2008JD011688, 2009.
406 Ren, X., van Duin, D., Cazorla, M., Chen, S., Mao, J., Zhang, L., Brune, W. H., Flynn, J. H.,
407 Grossberg, N., Lefer, B. L., Rappenglück, B., Wong, K. W., Tsai, C., Stutz, J., Dibb, J. E.,
408 Jobson, B. T., Luke, W. T., and Kelley, P.: Atmospheric oxidation chemistry and ozone
409 production: Results from SHARP 2009 in Houston, Texas, J. Geophys. Res., 118, 5770–5780,
410 2013.
411 Ryerson, T. B., et al., Effect of petrochemical industrial emissions of reactive alkenes and NOx
412 on tropospheric ozoneformation in Houston, Texas, J. Geophys. Res., 108(D8), 4249,
413 doi:10.1029/2002JD003070, 2003.
414 Sillman, S.: The use of NO_y, H_2O_2, and HNO_3 as indicators for O_3-NO_x-hydrocarbon sensitivity
415 in urban locations, J. Geophys. Res., 100, 14,175–14,188, 1995.
416 Sillman, S., Vautard, R., Menut, L., and Kley, D.: O_3-NO_x-VOC sensitivity and NO_x-VOC
417 indicators in Paris: Results from models and Atmospheric Pollution Over the Paris Area
418 (ESQUIF) measurements, J. Geophys. Res., 108(D17), 8563, doi:10.1029/2002JD001561,
419 2003.
420 Tang, X., Wang, Z., Zhu, J., Gbaguidi, A. E., Wu, Q., Li, J., and Zhu, T., Sensitivity of ozone to
421 precursor emissions in urban Beijing with a Monte Carlo scheme. Atmos. Environ., 44, 3833-
422 3842, 2010.
423 Thielmann, A., Pre´voˆt, A. S. H., and Staehelin, J.: Sensitivity of ozone production derived
424 from field measurements in theItalian Po basin, J. Geophys. Res., 107(D22), 8194,
425 doi:10.1029/2000JD000119, 2002.
426 Trainer, M., et al.: Correlation of ozone with NOy in photochemically aged air, J. Geophys. Res.,
427 98, 2917 – 2925, doi:10.1029/ 92JD01910, 1993.
428 Trainer, M., Parrish, D. D., Goldan, P. D., Roberts, J., and Fehsenfeld, F. C.: Review of
429 observation-based analysis of the regional factors influencing ozone concentrations, Atmos.
430 Environ., 34, 2045 – 2061, doi:10.1016/S1352-2310(99)00459-8, 2000.

Xue, L. K., Wang, T., Gao, J., Ding, A. J., Zhou, X. H., Blake, D. R., Wang, X. F., Saunders, S. M., Fan, S. J., Zuo, H. C., Zhang, Q. Z., and Wang, W. X.: Ozone production in four major cities of China: sensitivity to ozone precursors and heterogeneous processes, Atmos. Chem. Phys. Discuss., 13, 27,243–27,285, doi:10.5194/acpd-13-27243-2013, 2013.

Yarwood, G., Rao, S., Yocke, M., and Whitten, G. Z.: Updates to the Carbon Bond Mechanism: CB05, Final Report to the US EPA (RT-0400675),(http://www.camx.com/publ/pdfs/CB05_Final_Report_120805.pdf), 2005.

Zaveri, R. A., Berkowitz, C. M., Kleinman, L. I., Springston, S. R., Doskey, P. V., Lonneman, W. A., and Spicer, C. W.: Ozone production efficiency and NOx depletion in an urban plume: Interpretation of field observations and implications for evaluating O3-NOx-VOC sensitivity, J. Geophys. Res., 108(D14), 4436, doi:10.1029/2002JD003144, 2003.

443

444 **Table** 1. WRF and CMAQ model options that were used in both the original and improved
445 modeling scenarios.

Weather Research and Forecasting (WRF) Version 3.6.1 Model Options	
Radiation	Long Wave: Rapid Radiative Transfer Model (RRTM) Short Wave: Goddard
Surface Layer	Pleim-Xiu
Land Surface Model	Pleim-Xiu
Boundary Layer	Asymmetric Convective Model (ACM2)
Cumulus	Kain-Fritsch
Microphysics	WRF Single-Moment 6 (WSM-6)
Nudging	Observational and analysis nudging
Damping	Vertical velocity and gravity waves damped at top of modeling domain
SSTs	Multi-scale Ultra-high Resolution (MUR) SST analysis (~1 km resolution)
Meteorological Initial and Boundary Conditions and Analysis Nudging Inputs	NAM 12 km
Observational Nudging Inputs	NCEP ADP Global Surface and Upper Air Observational Weather Data
CMAQ Version 5.0.2 Model Options	
Chemical Mechanism	Carbon Bond (CB05)
Aerosol Module	Aerosols with aqueous extensions version 5 (AE5)
Dry deposition	M3DRY
Vertical diffusion	Asymmetric Convective Model 2 (ACM2)
Emissions	2012 TCEQ anthropogenic emissions Biogenic Emission Inventory System (BEIS) calculated within CMAQ
Chemical Initial and Boundary Conditions	Model for OZone and Related chemical Tracers (MOZART) Chemical Transport Model (CTM)

446

Figures:

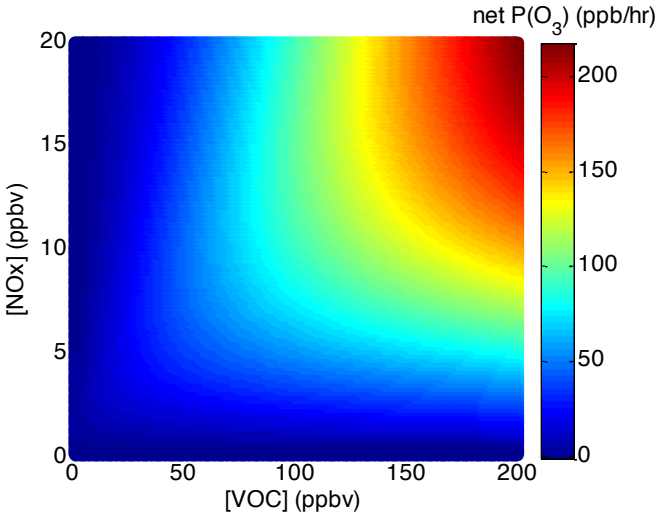

Figure 1. Ozone production empirical kinetic modeling approach (EKMA) diagram using a box model results with NOx levels varying from 0-20 ppbv and VOC levels from 0-200 ppbv while the mean concentrations of other species and the speciation of NOx and VOCs observed during DISCOVER-AQ in Houston in 2013 were used to constrain the box model. This diagram clearly shows the sensitivity of ozone production to NO_x and VOCs in Houston.

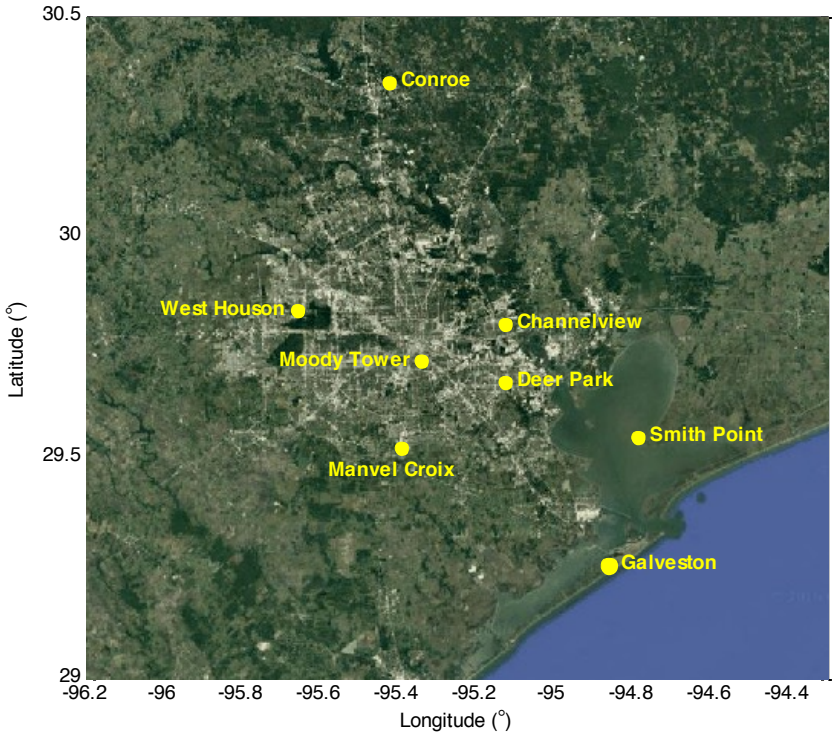

454

455

456 **Figure 2.** DISCOVER-AQ ground and spiral sites (yellow dots) during the September 2013
457 Houston campaign.

458

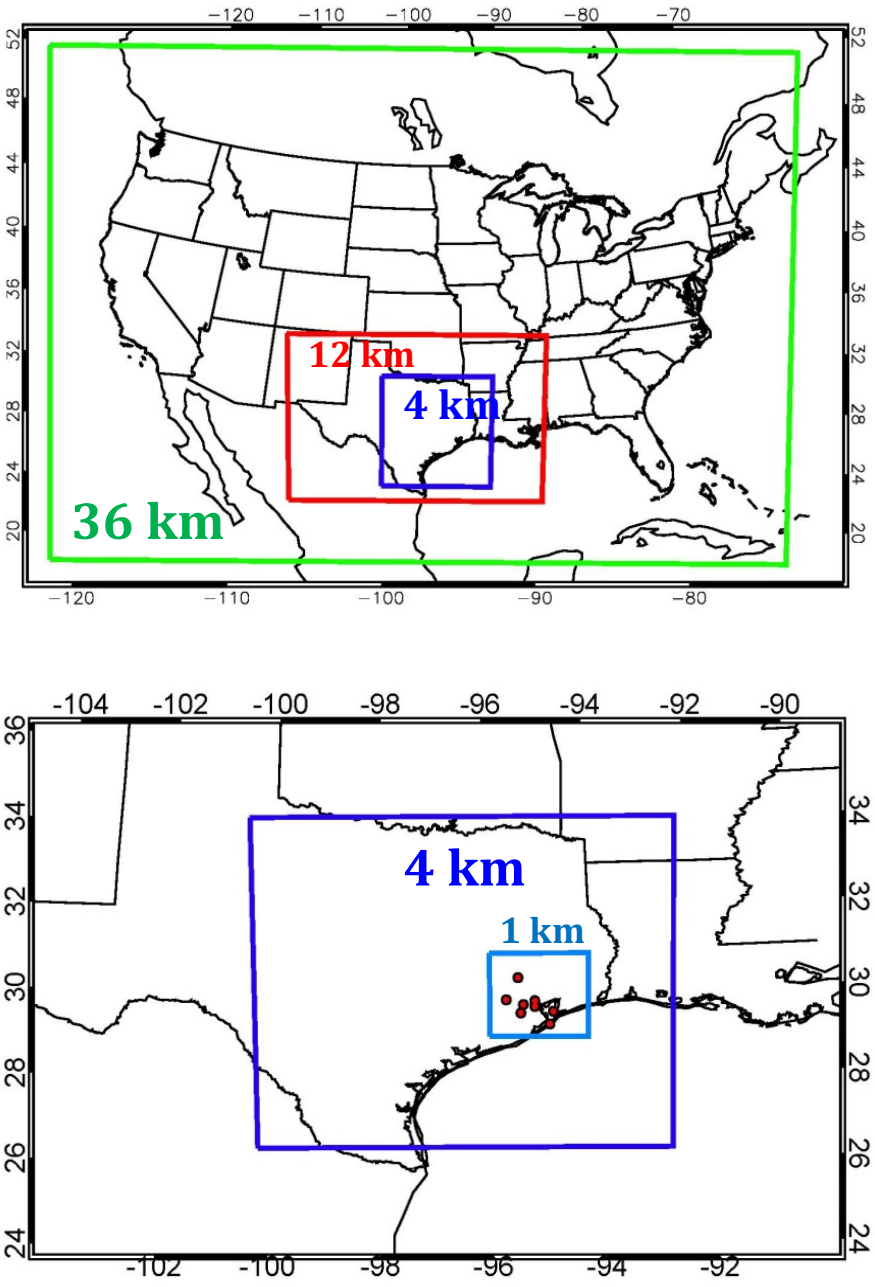

Figure 3. 36, 12, and 4 km CMAQ modeling domains (top); 4 and 1 km CMAQ modeling domains. The red dots show the NASA P-3B aircraft spiral locations (bottom).

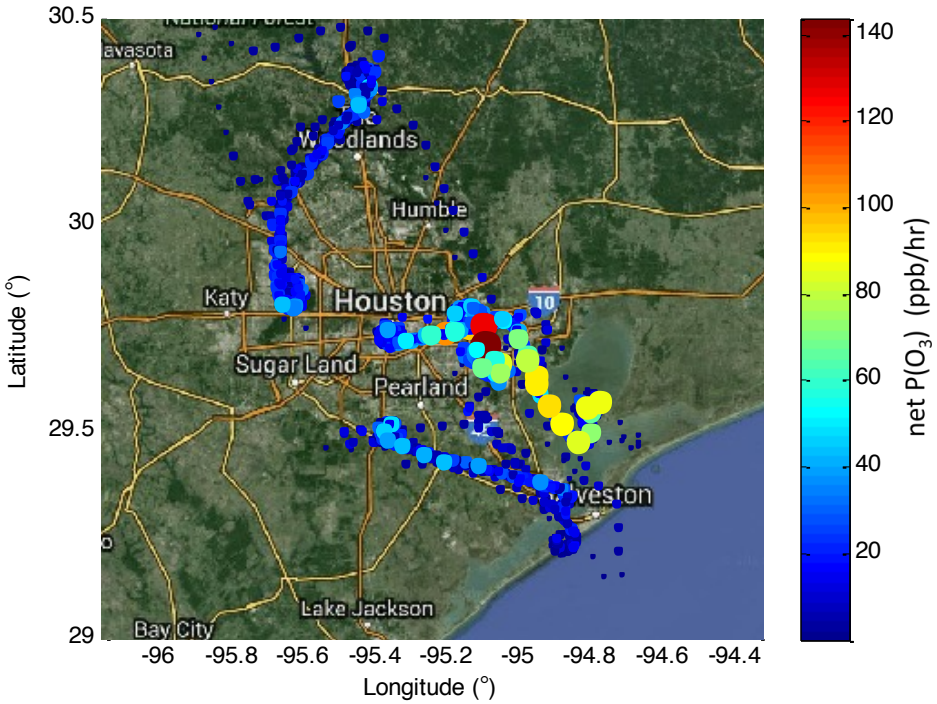

Figure 4. Net ozone production rate, net $P(O_3)$ calculated using the box model results along the P-3B flight track during DISCOVER-AQ in Houston in 2013. The size of dots is proportional to $P(O_3)$.

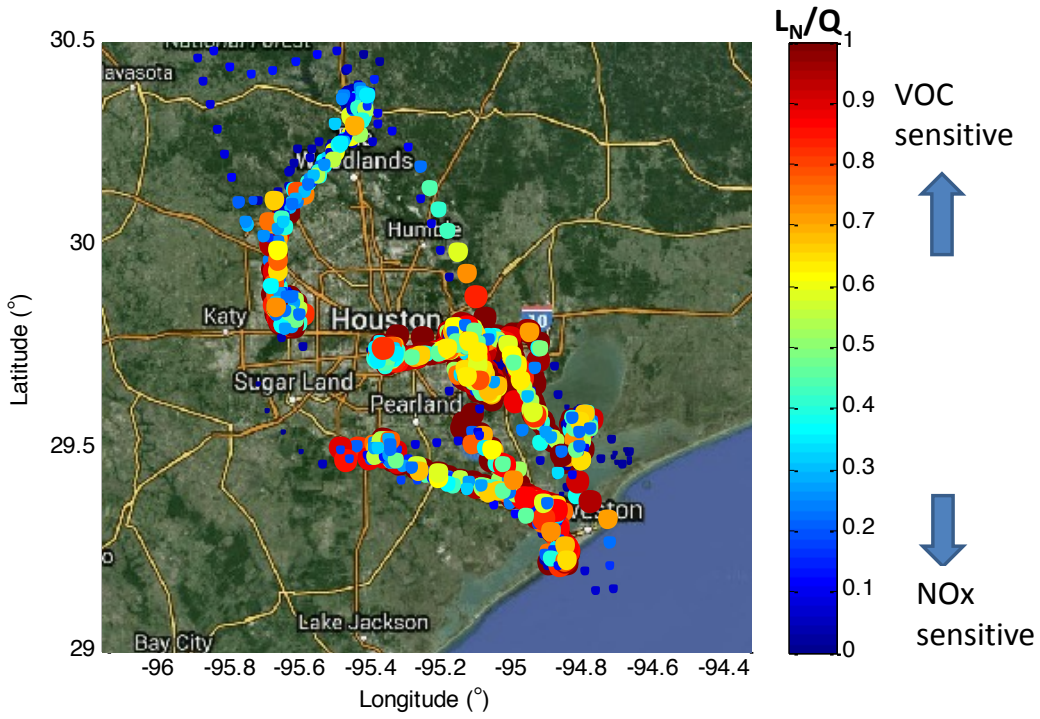

471

472 **Figure 5.** Ozone production sensitivity indicator, L_N/Q, along the P-3B flight track during
473 DISCOVER-AQ in Houston in 2013. $P(O_3)$ is VOC-sensitive when $L_N/Q > 0.5$, and NOx-
474 sensitive when $L_N/Q < 0.5$.

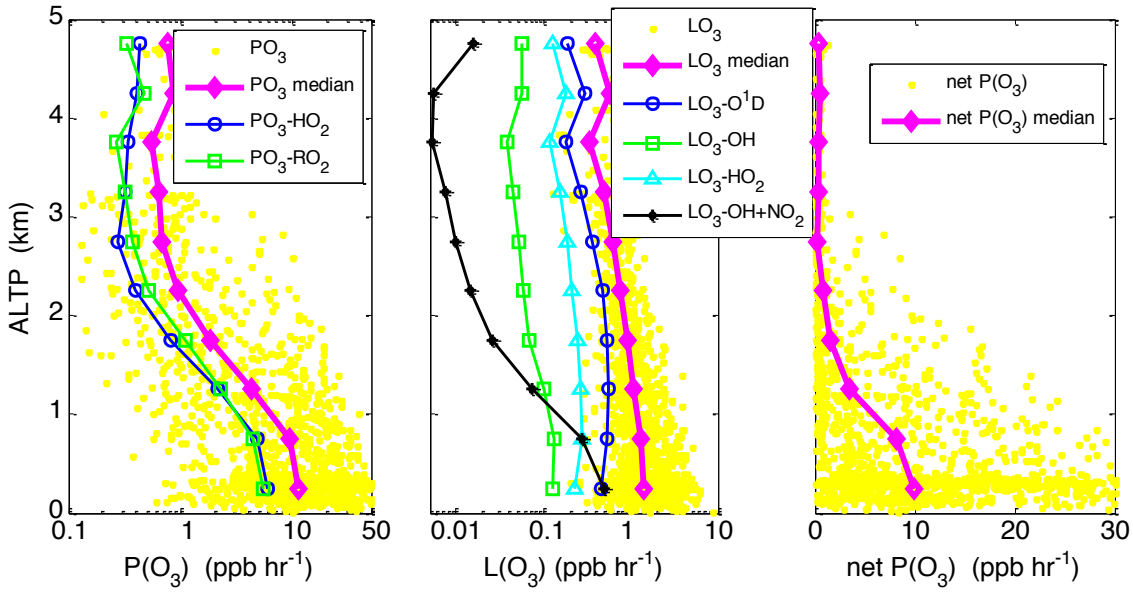

475

476 **Figure 6.** Vertical profiles of ozone production rate (left), ozone loss rate (middle), and net
477 ozone production rate (right) during DISCOVER-AQ in Houston in 2013.

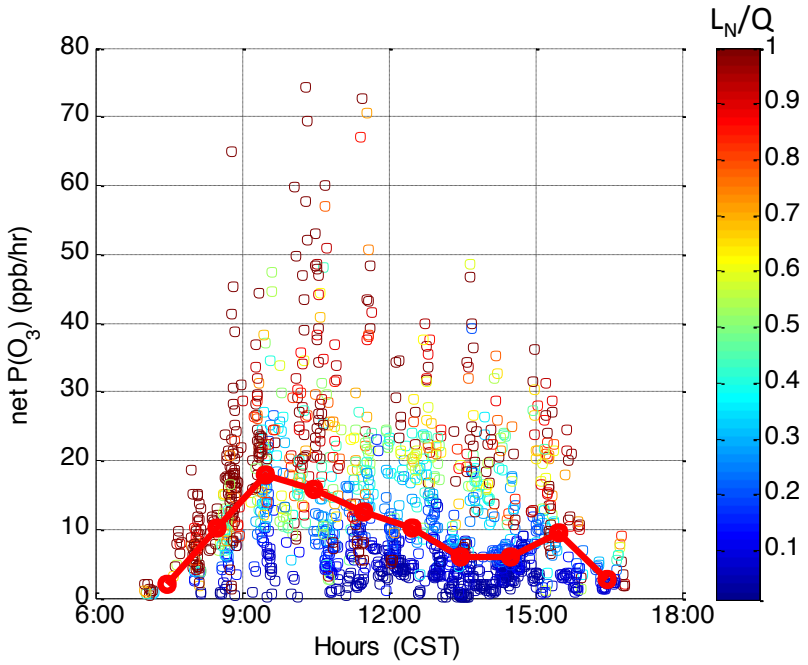

Figure 7. Diurnal variation of ozone production rate colored with the indicator L_N/Q on ten flight days during DISCOVER-AQ in Houston in 2013. The solid red circles represent the median values in hourly bins of $P(O_3)$. Data are limited with the pressure altitude less than 1000 m to represent the lowest layer of the atmosphere.

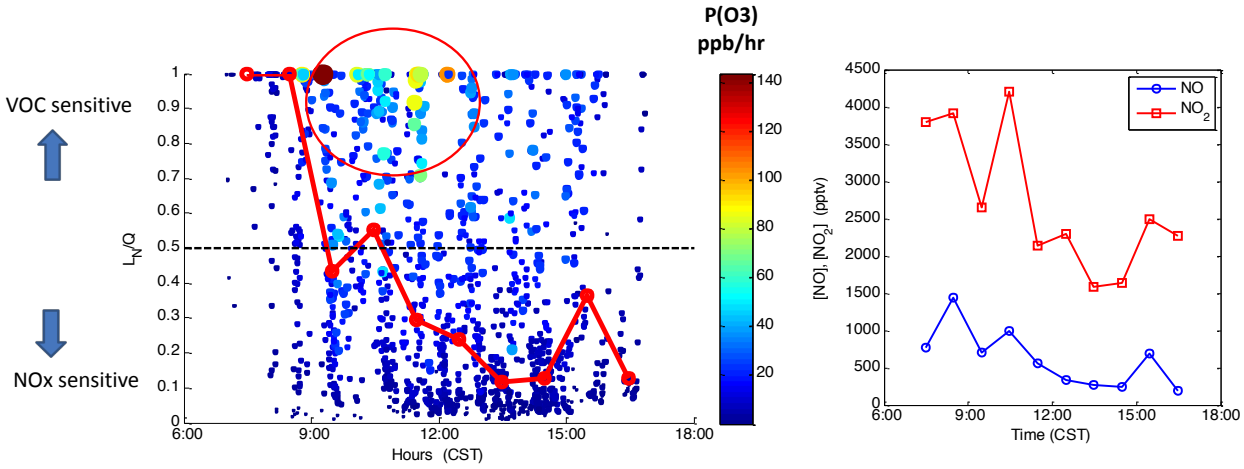

Figure 8. Diurnal variations of the indicator L_N/Q of ozone production rate sensitivity colored with ozone production rate and median hourly bins of L_N/Q shown in solid red circles (left) and median hourly NO and NO_2 concentrations (right) below 1000 m during DISCOVER-AQ in Houston in 2013.

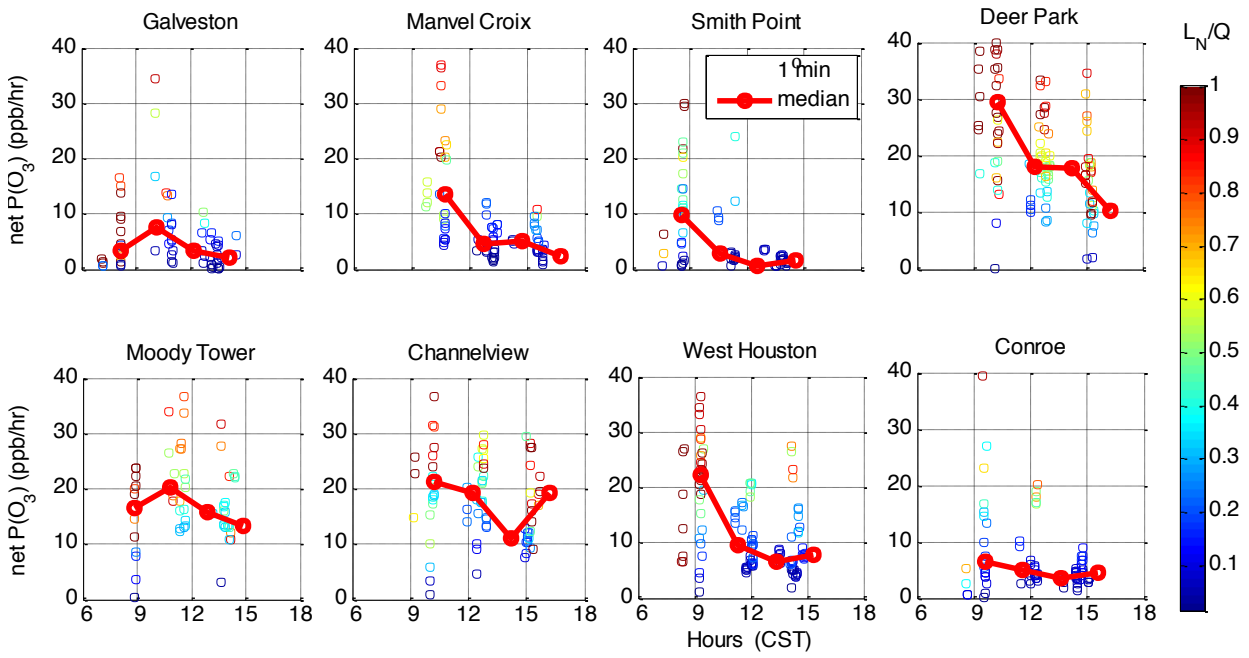

488

489 **Figure 9.** Diurnal variations of ozone production rate at eight individual spiral locations.
490 Individual points are 1-min data colored with L_N/Q and the linked red circles represent the
491 median values in hourly bins of $P(O_3)$. Data are limited with the pressure altitude less than 1000
492 m to represent the lowest layer of the atmosphere.

493

494

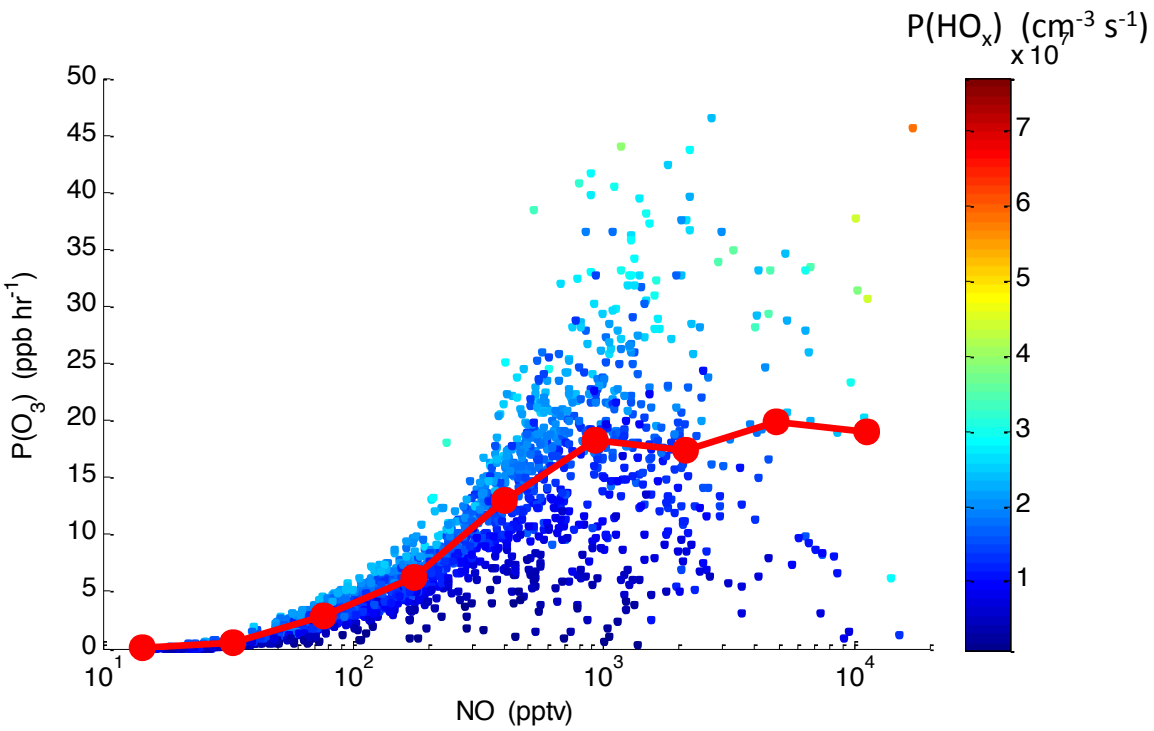

Figure 10. Ozone production as a function of NO mixing ratio. Individual data points are the 1-minute averages and are colored with the production rate of HOx (= OH + HO_2) during DISCOVER-AQ in Houston in 2013. The linked solid red circles represent the median values in [NO] bins. Note a log scale is used for the x-axis.

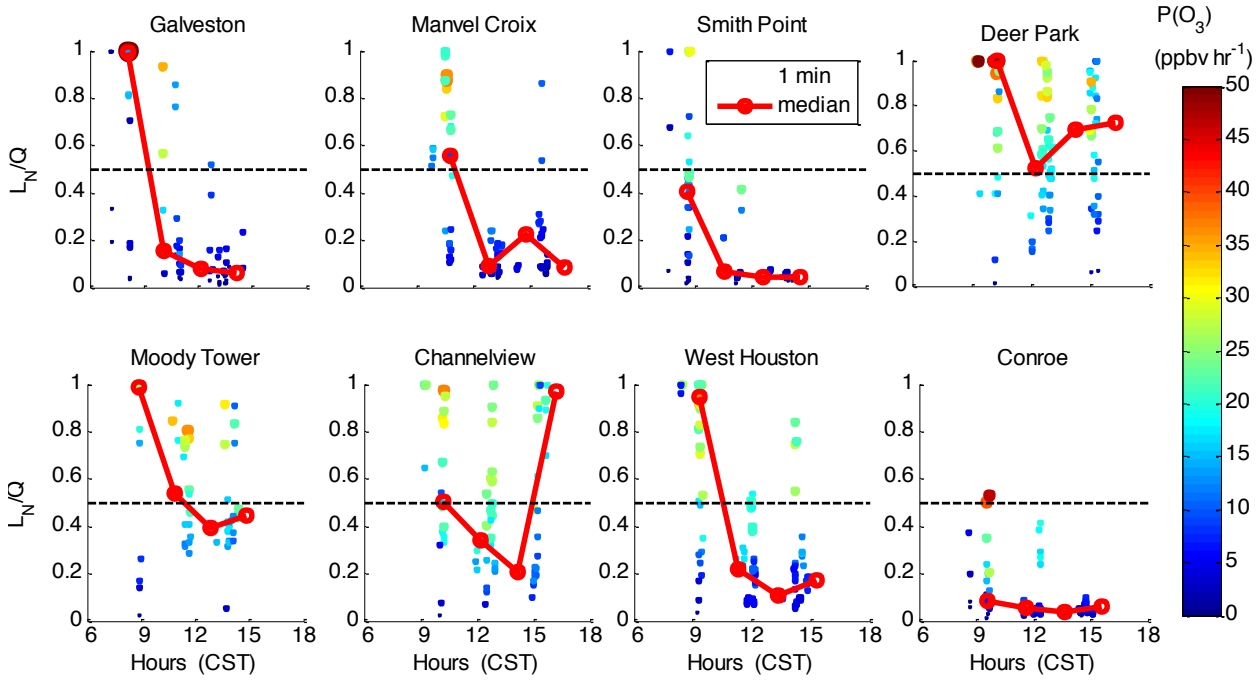

502

503 **Figure 11.** Diurnal variations of the indicator of ozone production sensitivity to NOx and VOCs,
504 L_N/Q, at eight individual spiral locations during DISCOVER-AQ in Houston in 2013. Individual
505 points are 1-min data colored by $P(O_3)$ and the linked red circles represent the median values in
506 hourly bins of $P(O_3)$. Data are limited with the pressure altitude less than 1000 m to represent the
507 lowest layer of the atmosphere.

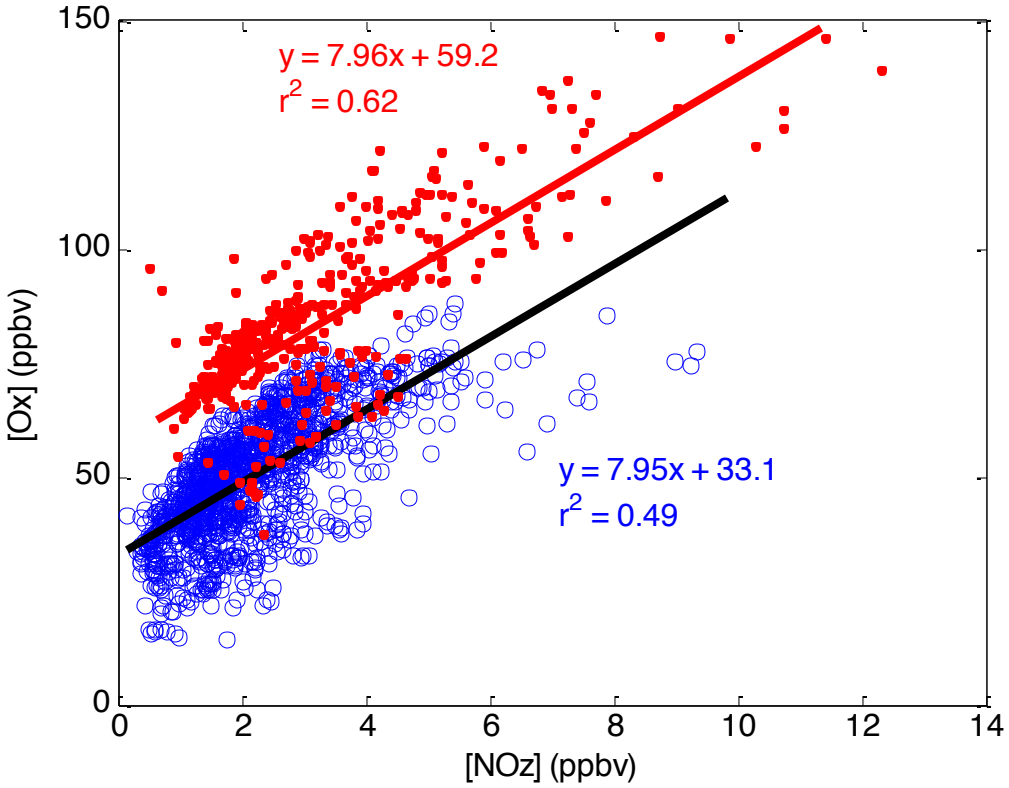

508

509 **Figure 12.** Photochemical oxidant, Ox (=O_3+NO_2) as a function of NOz (=NOy-NOx) during
510 DISCOVER-AQ in Houston in 2013. Red dots are the data collected on September 25 and 26,
511 2013 when high ambient ozone concentrations were observed. Blue circles are the data collected
512 during other flights. Data are limited with the pressure altitude less than 1000 m to represent the
513 lowest layer of the atmosphere.

514

515

516

517

518

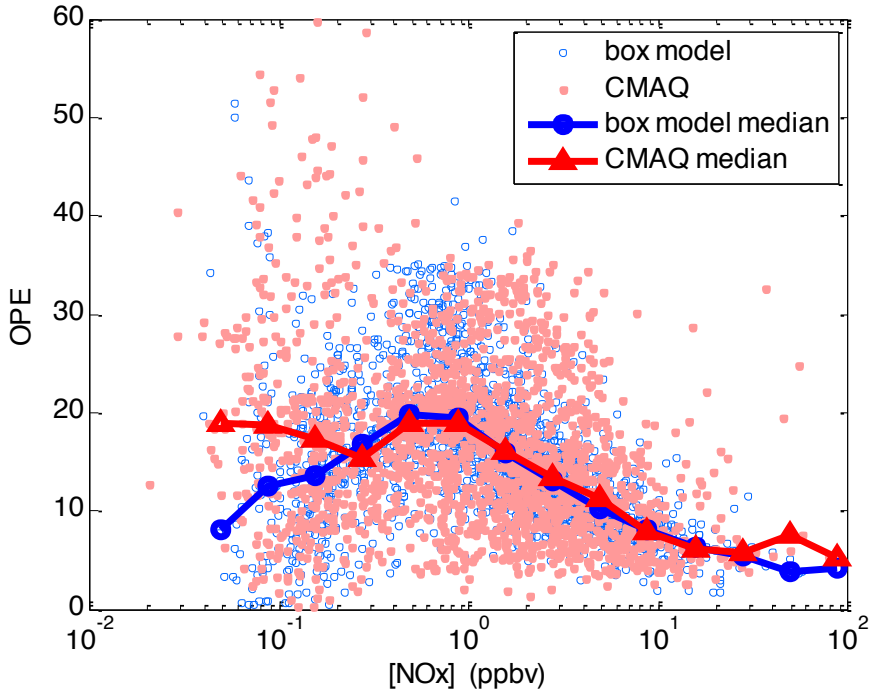

519

520 **Figure 13.** Ozone production efficiency (OPE) versus NOx in the box model (blue circles) and
521 CMAQ model (pink dots) results. The linked blue circles show the median OPE values binned
522 by NOx concentration in the box model, while the linked red triangles show the median OPE
523 values binned by NOx concentration in the CMAQ model, OPE is calculated according to its
524 definition as the net ozone formation rate divided by of the formation rate of NOz.

525

526

527

528

529

530

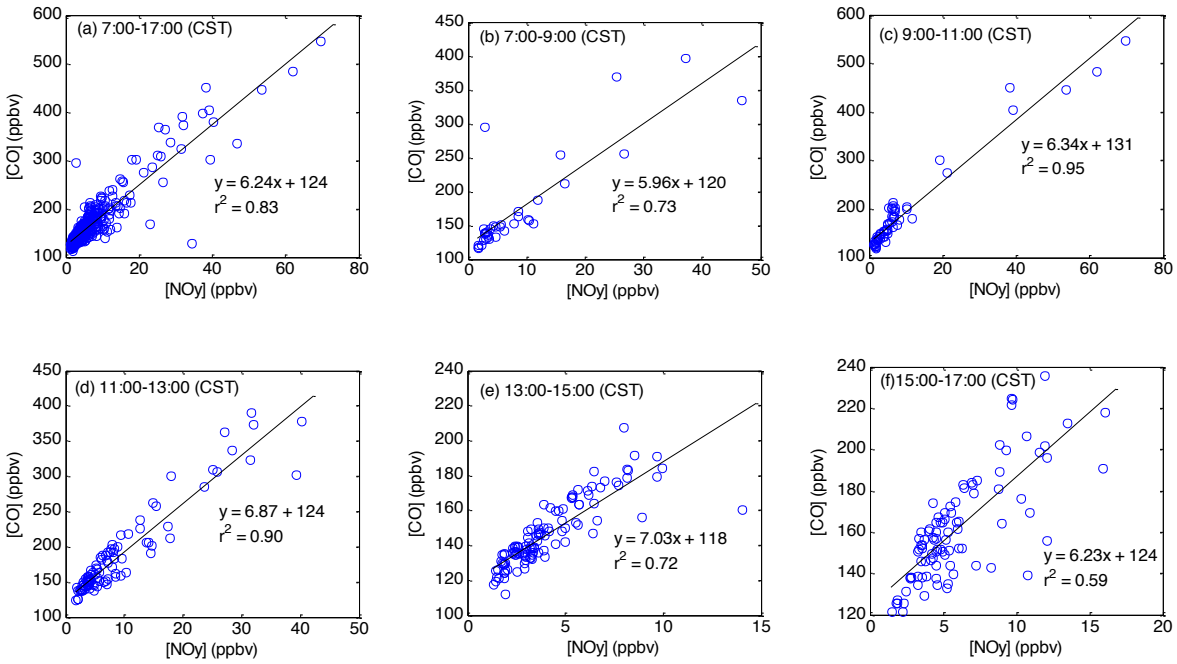

531

532 **Figure 14.** CO versus NOy and linear regression on September 25 and 26 at different times of
533 the day: (a) 07:00-17:00 (all data), (b) 07:00-09:00, (c) 09:00-11:00, (d) 11:00-13:00, (e) 13:00-
534 15:00, and (f) 15:00-17:00 (CST).

535

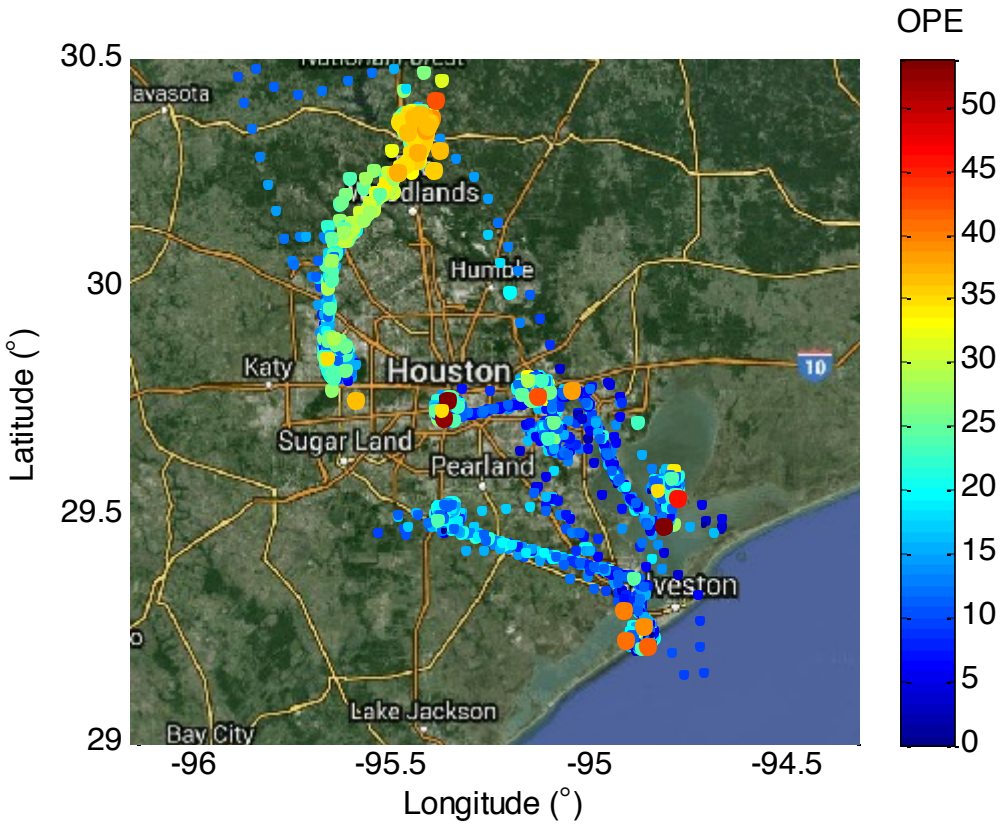

536

537 **Figure 15.** Ozone production efficiency (OPE) along the P-3B flight track during DISCOVER-
538 AQ in Houston in 2013. OPE was calculated using the box model results as the ratio of net ozone
539 formation rate to the formation rate of NO_z.

540

541